Radial distribution function of penetrable sphere fluids to second order in density

Andrés Santos[*]

Departamento de Física, Universidad de Extremadura, E-06071 Badajoz, Spain

Alexandr Malijevský[†]

E. Hála Laboratory of Thermodynamics, Academy of Science of the Czech Republic,
16502 Prague 6, Czech Republic and Institute of Theoretical Physics,
Faculty of Mathematics and Physics, Charles University, 18000 Prague 8, Czech Republic

(Dated: February 6, 2008)

The simplest bounded potential is that of penetrable spheres, which takes a positive finite value ϵ if the two spheres are overlapped, being 0 otherwise. In this paper we derive the cavity function to second order in density and the fourth virial coefficient as functions of $T^* \equiv k_B T/\epsilon$ (where k_B is the Boltzmann constant and T is the temperature) for penetrable sphere fluids. The expressions are exact, except for the function represented by an elementary diagram inside the core, which is approximated by a polynomial form in excellent agreement with accurate results obtained by Monte Carlo integration. Comparison with the hypernetted-chain (HNC) and Percus–Yevick (PY) theories shows that the latter is better than the former for $T^* \lesssim 1$ only. However, even at zero temperature (hard sphere limit), the PY solution is not accurate inside the overlapping region, where no practical cancelation of the neglected diagrams takes place. The exact fourth virial coefficient is positive for $T^* \lesssim 0.73$, reaches a minimum negative value at $T^* \approx 1.1$, and then goes to zero from below as $1/T^{*4}$ for high temperatures. These features are captured qualitatively, but not quantitatively, by the HNC and PY predictions. In addition, in both theories the compressibility route is the best one for $T^* \lesssim 0.7$, while the virial route is preferable if $T^* \gtrsim 0.7$.

PACS numbers: 61.20.Gy, 61.20.Ne, 05.20.Jj, 05.70.Ce

I. INTRODUCTION

Ultrasoft and bounded potentials represent useful models to characterize the effective two-body interaction in some colloidal systems, such as star or chain polymers in good solvents [1, 2, 3, 4, 5, 6, 7, 8]. The simplest bounded potential is that of so-called penetrable spheres (PS), which is defined as

$$\phi(r) = \begin{cases} \epsilon, & r < \sigma, \\ 0, & r > \sigma, \end{cases} \qquad (1.1)$$

where $\epsilon > 0$. This interaction potential was suggested by Marquest and Witten [9] as a simple theoretical approach to the explanation of the experimentally observed crystallization of copolymer mesophases and it has been since then the subject of a number of studies [7, 10, 11, 12, 13, 14, 15, 16, 17, 18, 19, 20, 21]. The classical integral equation theories, in particular the Percus–Yevick (PY) and the hypernetted-chain (HNC) approximations, do not describe satisfactorily well the structure of the PS fluid, especially inside the overlapping region for low temperatures. Thus, the PS model can be used as a stringent benchmark to test alternative theories [12, 13, 14, 17, 21]. From that point of view, the derivation of exact properties provides an invaluable tool. The exact structural and thermodynamic

properties of the PS fluid in the high-temperature limit $T^* \equiv k_B T/\epsilon \to \infty$ (where k_B is the Boltzmann constant and T is the temperature) are known for any density $\rho\sigma^3$, including the high-density regime $\rho\sigma^3 \sim T^*$ [18]. On the other hand, the corresponding properties in the complementary low-density limit for any temperature has not been addressed, to the best of our knowledge, except in the one-dimensional case [21].

The aim of this paper is to derive the exact expressions for the radial distribution function $g(r)$ and, equivalently, the cavity function $y(r)$ of PS fluids to second order in density. To that end we will exploit the fact that the PS Mayer function is proportional to the hard sphere (HS) Mayer function. This implies that the diagrams to be evaluated are the same as in the case of HS, except that now each diagram is affected by a temperature-dependent factor.

In the next Section we present some definitions and basic equations. The density expansion of $y(r)$ to second order is worked out in Sec. III, where the HS functions derived by Nijboer and van Hove [22] outside the core $r > \sigma$ are complemented by their extensions in the overlapping region ($r < \sigma$). However, we have not been able to derive the rigorously exact expression for $r < \sigma$ of the function $\chi(r)$ represented by the only elementary diagram. Instead, the exact values of $\chi(0)$, $\chi'(0)$, $\chi(\sigma)$, $\chi'(\sigma)$, $\chi''(\sigma)$, $\chi'''(\sigma)$, and $\int_0^\sigma dr\, r^2\chi(r)$ are obtained in Sec. IV. With these constraints, we have constructed a polynomial approximation of $\chi(r)$ for $r < \sigma$ which yields results indistinguishable from those obtained by Monte Carlo (MC) integration with six significant figures. The

[*]Electronic address: andres@unex.es; URL: http://www.unex.es/eweb/fisteor/andres/
[†]Electronic address: malijevsky@icpf.cas.cz

exact fourth virial coefficient is also derived in Sec. IV. The exact results are compared with the HNC and PY predictions in Sec. V. It is seen that the latter is generally preferable at low temperatures, while the former is more accurate at high temperatures. The paper ends with the conclusion section.

II. DEFINITIONS AND BASIC EQUATIONS

We consider in this paper a fluid of particles interacting via the pairwise potential (1.1). Henceforth we take $\sigma = 1$ as the length unit. Let us introduce the cavity (or background) function

$$y(r|\eta, T^*) = e^{\phi(r)/k_B T} g(r|\eta, T^*), \qquad (2.1)$$

where $g(r|\eta, T^*)$ is the radial distribution function, $\eta \equiv (\pi/6)\rho$ being the packing fraction. Equation (2.1) implies that

$$g(r|\eta, T^*) = y(r|\eta, T^*) - xy(r|\eta, T^*)\Theta(1 - r), \quad (2.2)$$

where $\Theta(r)$ is the Heaviside step function and we have called

$$x \equiv 1 - e^{-1/T^*}. \qquad (2.3)$$

The parameter x represents the probability of rejecting an overlap of two particles in a MC move. The thermodynamic quantities can be expressed in terms of $g(r|\eta, T^*)$ or $y(r|\eta, T^*)$ [23, 24, 25]. Particularized to the PS model, the compressibility factor $Z \equiv p/\rho k_B T$ is given by the virial equation of state as

$$Z(\eta, T^*) = 1 + 4\eta x y(1|\eta, T^*). \qquad (2.4)$$

The (dimensionless) isothermal compressibility $K \equiv k_B T \left(\partial \rho / \partial p\right)_T$ is

$$K(\eta, T^*) = 1 + 24\eta \left\{ \int_0^\infty dr\, r^2 \left[y(r|\eta, T^*) - 1\right] \right.$$
$$\left. - x \int_0^1 dr\, r^2 y(r|\eta, T^*) \right\}. \qquad (2.5)$$

Finally, the internal energy per particle can be written as

$$u(\eta, T^*) = \epsilon \left[\frac{3}{2} T^* + 12\eta(1 - x) \int_0^1 dr\, r^2 y(r|\eta, T^*) \right]. \qquad (2.6)$$

These three quantities are thermodynamically connected by the relations

$$K^{-1} = \frac{\partial(\eta Z)}{\partial \eta}, \qquad (2.7)$$

$$\eta \frac{\partial(u/\epsilon)}{\partial \eta} = (1 - x)\frac{\partial Z}{\partial x}. \qquad (2.8)$$

The series expansions of the cavity function and the compressibility factor in powers of density read

$$y(r|\eta, T^*) = 1 + \sum_{n=1}^\infty y_n(r|T^*) \left(\frac{6}{\pi}\right)^n \eta^n, \qquad (2.9)$$

$$Z(\eta, T^*) = 1 + \sum_{n=1}^\infty b_{n+1}(T^*)\eta^n. \qquad (2.10)$$

In Eq. (2.10), $b_n(T^*)$ is the (reduced) nth virial coefficient. The quantities $\{b_n(T^*)\}$ can be obtained from the functions $\{y_n(r|T^*)\}$ through the virial route, Eq. (2.4), the compressibility route, Eq. (2.5), or the energy route, Eq. (2.6). In order to distinguish the results derived through each route, we will use the notation $b_n^v(T^*)$, $b_n^c(T^*)$, $b_n^e(T^*)$, respectively. Of course, $b_n^v(T^*) = b_n^c(T^*) = b_n^e(T^*)$ if the exact cavity function is employed.

Insertion of the expansion (2.9) into Eqs. (2.4) and (2.6) yields (for $n \geq 2$)

$$b_n^v(T^*) = 4x \left(\frac{6}{\pi}\right)^{n-2} y_{n-2}(1|T^*), \qquad (2.11)$$

$$b_n^e(T^*) = 12(n - 1) \left(\frac{6}{\pi}\right)^{n-2} \int_0^x dx_1 \int_0^1 dr\, r^2 y_{n-2}(r|T_1^*). \qquad (2.12)$$

In Eq. (2.12) use has been made of Eq. (2.8) and of the ideal gas condition $\lim_{T^* \to \infty} b_n(T^*) = 0$. In the case of the compressibility route, insertion of Eq. (2.9) into Eq. (2.5) and use of the relation (2.7) leads to the recursive formula

$$b_n^c(T^*) = -\sum_{m=1}^{n-1} \frac{m}{n} b_m^c(T^*) K_{n-m}(T^*), \qquad (2.13)$$

where $K_1(T^*) = -8x$ and

$$K_n(T^*) \equiv 24 \left(\frac{6}{\pi}\right)^{n-1} \left[\int_0^\infty dr\, r^2 y_{n-1}(r|T^*) \right.$$
$$\left. - x \int_0^1 dr\, r^2 y_{n-1}(r|T^*) \right] \qquad (2.14)$$

for $n \geq 2$.

III. CAVITY FUNCTION TO SECOND ORDER IN DENSITY

The virial coefficients $y_n(r|T^*)$ are represented by diagrams [23, 25]. In particular,

$$y_1(r|T^*) = \qquad\qquad , \qquad (3.1)$$

$$y_2(r|T^*) \; = \quad \text{[diagram]} \; + 2 \, \text{[diagram]} \; + \frac{1}{2} \, \text{[diagram]}$$

$$+ \frac{1}{2} \, \text{[diagram]} . \tag{3.2}$$

Here, the open circles represent *root* points separated by a distance r, the filled circles represent *field* points to be integrated out, and each bond represents a Mayer function

$$f(r|T^*) = e^{-\phi(r)/k_B T} - 1. \tag{3.3}$$

Thus, for instance,

$$\text{[diagram, vertices 1, 2, 3]} = \int d\mathbf{r}_3 \, f(r_{13}|T^*) f(r_{23}|T^*), \tag{3.4}$$

$$\text{[diagram, vertices 1, 2, 3, 4]} = \int d\mathbf{r}_3 \int d\mathbf{r}_4 \, f(r_{13}|T^*) f(r_{34}|T^*)$$
$$\times f(r_{24}|T^*) f(r_{14}|T^*), \tag{3.5}$$

where $r_{ij} = |\mathbf{r}_i - \mathbf{r}_j|$ and $r_{12} = r$.

Equations (3.1)–(3.5) hold for any interaction potential. In the special case of PS, the Mayer function becomes

$$f(r|T^*) = x f_{\text{HS}}(r), \tag{3.6}$$

where

$$f_{\text{HS}}(r) = -\Theta(1 - r) \tag{3.7}$$

is the Mayer function of HS. Therefore, the spatial dependence of each one of the diagrams contributing to the virial expansion (2.9) is exactly the same as for HS. The only difference is that each diagram is now multiplied by the temperature-dependent parameter x raised to a power equal to the number of bonds in that particular diagram. As a consequence, Eqs. (3.1) and (3.2) become

$$y_1(r|T^*) = x^2 \gamma(r), \tag{3.8}$$

$$y_2(r|T^*) = x^3 \varphi(r) + 2x^4 \psi(r) + \frac{x^4}{2} \gamma^2(r) + \frac{x^5}{2} \chi(r). \tag{3.9}$$

Here, $\gamma(r)$ is represented by the diagram on the right-hand side of Eq. (3.1), except that now each bond corresponds to a Mayer function f_{HS}. Analogously, the functions $\varphi(r)$, $\psi(r)$, and $\chi(r)$ are represented by the first,

second, and fourth diagram, respectively, on the right-hand side of Eq. (3.2), with f_{HS} for each bond. The expressions of these functions for $r > 1$ are known [22, 26]. The region $r > 1$ is the physically relevant one in the case of HS. However, the overlapping region $r < 1$ is essential in the case of PS, since $g(r|\eta, T^*) \neq 0$ for $r < 1$, except in the zero-temperature limit (where the PS model reduces to the HS one). Therefore, it is necessary to extend the knowledge of $\gamma(r)$, $\varphi(r)$, $\psi(r)$, and $\chi(r)$ to the domain $0 \leq r \leq 1$.

Given a radial function $F(r)$ we define its Fourier transform as

$$\widetilde{F}(k) = \int d\mathbf{r} \, e^{i\mathbf{k} \cdot \mathbf{r}} F(r) = \frac{4\pi}{k} \int_0^\infty dr \, r \sin(kr) F(r). \tag{3.10}$$

It is easy to realize that $\widetilde{\gamma}(k) = [\widetilde{f}_{\text{HS}}(k)]^2$, where

$$\widetilde{f}_{\text{HS}}(k) = 4\pi \frac{k \cos k - \sin k}{k^3}. \tag{3.11}$$

Inverse Fourier transform simply yields

$$\gamma(r) = \frac{\pi}{12} (2 - r)^2 (r + 4) \Theta(2 - r). \tag{3.12}$$

This implies that the function $\gamma(r)$ for $0 \leq r \leq 1$ is just the analytical continuation of its expression for $1 \leq r \leq 2$. Next, note that $\widetilde{\varphi}(k) = [\widetilde{f}_{\text{HS}}(k)]^3$, so that

$$\varphi(r) = \varphi_A(r) \Theta(1 - r) + \varphi_B(r) \Theta(3 - r) \tag{3.13}$$

with

$$\varphi_A(r) = \frac{\pi^2}{36} \frac{3}{35r} (r - 1)^4 (r^3 + 4r^2 - 53r - 162), \tag{3.14}$$

$$\varphi_B(r) = -\frac{\pi^2}{36} \frac{1}{35r} (r - 3)^4 (r^3 + 12r^2 + 27r - 6). \tag{3.15}$$

Therefore, $\varphi(r) = \varphi_A(r) + \varphi_B(r)$ for $0 \leq r \leq 1$, while $\varphi(r) = \varphi_B(r)$ for $1 \leq r \leq 3$. In the case of $\psi(r)$, one has $\widetilde{\psi}(k) = \widetilde{f}_{\text{HS}}(k) \widetilde{\gamma}^*(k)$, where $\gamma^*(r) = \gamma(r) f_{\text{HS}}(r)$. As a consequence,

$$\psi(r) = \psi_A(r) \Theta(1 - r) + \psi_B(r) \Theta(2 - r) \tag{3.16}$$

with

$$\psi_A(r) = -\frac{2}{3} \varphi_A(r), \tag{3.17}$$

$$\psi_B(r) = \frac{\pi^2}{36} \frac{1}{35r} (r - 2)^2 (r^5 + 4r^4 - 51r^3 - 10r^2 + 479r - 81). \tag{3.18}$$

Equations (3.15) and (3.18) coincide with those derived in Ref. [22] by a different method. On the other hand, the functions $\varphi_A(r)$ and $\psi_A(r)$, which are needed to get $\varphi(r < 1)$ and $\psi(r < 1)$, respectively, were not considered in Refs. [22] and [26]. Near the origin,

$$\gamma(r) = \frac{\pi}{6} (8 - 6r) + \mathcal{O}(r^2), \tag{3.19}$$

$$\varphi(r) = -\frac{\pi^2}{36}30 + \mathcal{O}(r^2), \qquad (3.20)$$

$$\psi(r) = \frac{\pi^2}{36}\left(30 - 15r\right) + \mathcal{O}(r^2). \qquad (3.21)$$

Equations (3.13)–(3.18) show that $\varphi(r)$ has a fourth-order discontinuity at $r = 1$ and at $r = 3$, while $\psi(r)$ has a fourth-order discontinuity at $r = 1$ and a second-order discontinuity at $r = 2$.

Now we turn to the much more involved function $\chi(r)$, represented by the elementary diagram at the end of the right-hand side of Eq. (3.2). Let us decompose it in a form similar to Eqs. (3.13) and (3.16),

$$\chi(r) = \chi_A(r)\Theta(1-r) + \chi_B(r)\Theta(\sqrt{3}-r) - \gamma^2(r). \quad (3.22)$$

The exact expression for $\chi_B(r)$ was obtained by Nijboer and van Hove [22]. It reads

$$
\begin{aligned}
\chi_B(r) \;=\; & \pi\left[-r^2\left(\frac{3r^2}{280} - \frac{41}{420}\right)\sqrt{3-r^2} - \left(\frac{23}{15}r - \frac{36}{35r}\right)\right.\\
& \times \cos^{-1}\frac{r}{\sqrt{3(4-r^2)}} + \left(\frac{3r^6}{560} - \frac{r^4}{15} + \frac{r^2}{2} + \frac{2r}{15}\right.\\
& \left.- \frac{9}{35r}\right)\cos^{-1}\frac{r^2 + r - 3}{\sqrt{3(4-r^2)}} + \left(\frac{3r^6}{560} - \frac{r^4}{15}\right.\\
& \left.\left.+ \frac{r^2}{2} - \frac{2r}{15} + \frac{9}{35r}\right)\cos^{-1}\frac{-r^2 + r + 3}{\sqrt{3(4-r^2)}}\right]. \quad (3.23)
\end{aligned}
$$

We have not been able to obtain an analytic expression for $\chi(r)$ in the interval $0 \le r \le 1$. By working with bipolar coordinates, it is possible to express the derivative $\chi'(r < 1)$ as a sum of 13 triple integrals, but only two of them seem to be analytically solvable. Therefore, we have resorted to numerical evaluation of $\chi(r < 1)$ by the MC method [26] and to a very accurate polynomial approximation. In order to construct the latter, some constraints on the exact $\chi(r < 1)$ are derived in the next Section.

IV. CONSTRAINTS ON $\chi(r)$. POLYNOMIAL APPROXIMATION

In this Section we derive some constraints on $\chi(r)$ for $r \le 1$. First, we take into account that $\chi(r)$ and its first three derivatives must be continuous at $r = 1$. We are not aware of a formal proof of this statement, but it is strongly supported by the following two arguments: (i) both $\varphi(r)$ and $\psi(r)$ have a fourth-order discontinuity at $r = 1$, even though a diagonal bond is added when going from the diagram representing $\varphi(r)$ to that representing $\psi(r)$; (ii) in the one-dimensional case, the three functions $\varphi(r)$, $\psi(r)$, and $\chi(r)$ have the same type of singularity at $r = 1$, namely a second-order discontinuity [21].

From Eqs. (3.22) and (3.23) one can get

$$\chi(1) = \frac{\pi^2}{36}\left(\frac{b_4^{\mathrm{HS}}}{2} - \frac{57}{4}\right), \qquad (4.1)$$

$$\chi'(1) = \frac{\pi^2}{36}\frac{1}{51}\left(\frac{347 b_4^{\mathrm{HS}}}{3} - \frac{7219}{6} - \frac{256\sqrt{2}}{\pi}\right), \quad (4.2)$$

$$\chi''(1) = \frac{\pi^2}{36}\frac{1}{153}\left(-\frac{619 b_4^{\mathrm{HS}}}{3} - \frac{8149}{6} + \frac{2432\sqrt{2}}{\pi}\right), \quad (4.3)$$

$$\chi'''(1) = \frac{\pi^2}{36}\frac{2}{153}\left(\frac{946 b_4^{\mathrm{HS}}}{3} - \frac{16597}{3} - \frac{4832\sqrt{2}}{\pi}\right). \quad (4.4)$$

In the above equations,

$$b_4^{\mathrm{HS}} = \frac{2707}{70} + \frac{438\sqrt{2} - 4131\sec^{-1}3}{70\pi} \simeq 18.3648 \quad (4.5)$$

is the exact value of the fourth virial coefficient for HS.

Next, note that

$$
\begin{aligned}
\chi(0) &= \int d\mathbf{r}\,\gamma(r)f_{\mathrm{HS}}(r) = -\frac{\pi^2}{3}\int_0^1 dr\, r^2(r-2)^2(r+4)\\
&= -\frac{\pi^2}{36}30. \qquad (4.6)
\end{aligned}
$$

The same result is obtained from the following zero-separation theorem for HS [27]:

$$\ln y_{\mathrm{HS}}(0|\eta) = 4\eta y_{\mathrm{HS}}(1|\eta) + 4\int_0^\eta d\eta_1 y_{\mathrm{HS}}(1|\eta_1), \quad (4.7)$$

where $y_{\mathrm{HS}}(r|\eta) = \lim_{T^*\to 0} y(r|\eta, T^*)$ is the cavity function for HS. As a further constraint on the unknown function $\chi(r)$ for $r < 1$, let us consider the alternative zero-separation theorem

$$\frac{y'_{\mathrm{HS}}(0|\eta)}{y_{\mathrm{HS}}(0|\eta)} = -6\eta y_{\mathrm{HS}}(1|\eta). \qquad (4.8)$$

This implies that $\lim_{T^*\to 0} y'_2(0|T^*) = -(\pi^2/36)63$. From Eqs. (3.9) and (3.19)–(3.21) one then has

$$\chi'(0) = \frac{\pi^2}{36}30. \qquad (4.9)$$

As a consequence of Eqs. (3.19)–(3.21), (4.6), and (4.9), the form of y_2 near the origin is

$$
\begin{aligned}
y_2(r|T^*) \;=\; & \frac{\pi^2}{36}x^3\left[-30 + 2x(46 - 39r) - 15x^2(1-r)\right]\\
& + \mathcal{O}(r^2). \qquad (4.10)
\end{aligned}
$$

Let us apply now the condition of thermodynamic consistency for the fourth virial coefficient $b_4(T^*)$. Taking

into account that $y_0(r|T^*) = 1$, $y_1(1|T^*) = x^2\gamma(1) = (5\pi/12)x^2$, and

$$
\begin{aligned}
y_2(1|T^*) &= x^3\varphi(1) + 2x^4\psi(1) + \frac{x^4}{2}\gamma^2(1) + \frac{x^5}{2}\chi(1) \\
&= \frac{\pi^2}{36}x^3\left[-\frac{544}{35} + \frac{6347}{280}x + \left(\frac{b_4^{\mathrm{HS}}}{4} - \frac{57}{8}\right)x^2\right],
\end{aligned}
$$
(4.11)

Eq. (2.11) yields

$$
b_2(T^*) = 4x, \quad b_3(T^*) = 10x^3, \tag{4.12}
$$

$$
b_4(T^*) = x^4\left[b_4^{\mathrm{HS}}x^2 - (1-x)\frac{4352 - 1995x}{70}\right]. \tag{4.13}
$$

The same results for b_2 and b_3 are obtained through the energy route, Eq. (2.12). As for b_4, Eq. (2.12) yields

$$
\begin{aligned}
b_4(T^*) &= \frac{36}{\pi^2}9x^4\int_0^1 dr\, r^2\left[\varphi(r) + \frac{8}{5}x\psi(r)\right.\\
&\left.+\frac{2}{5}x\gamma^2(r) + \frac{1}{3}x^2\chi(r)\right].
\end{aligned}
$$
(4.14)

Since the functions $\varphi(r)$, $\psi(r)$, and $\gamma^2(r)$ are known for $r < 1$, the integrals involving them can be performed. Thus, equating the right-hand sides of Eqs. (4.13) and (4.14) one gets

$$
\int_0^1 dr\, r^2\chi(r) = \frac{\pi^2}{36}\left(\frac{b_4^{\mathrm{HS}}}{3} - \frac{57}{6}\right) = \frac{2}{3}\chi(1). \tag{4.15}
$$

In turn, this condition implies that

$$
K_3 = -2x^3\left[256 - \frac{12752}{35}x + \frac{6347}{35}x^2 + \left(2b_4^{\mathrm{HS}} - 57\right)x^3\right],
$$
(4.16)

where the coefficients K_n are defined by Eq. (2.14). Use of $K_1 = -8x$, $K_2 = 2x^2(32 - 15x)$, and (4.16) in Eq. (2.13) leads again to Eqs. (4.12) and (4.13) [28].

Although the exact analytic expression of $\chi_A(r)$, and hence of $\chi(r)$ for $r < 1$ is not known, we have derived in this Section a number of constraints. The value of $\chi(r)$ and its first three derivatives at $r = 1$ are given by Eqs. (4.1)–(4.4). On the other hand, Eqs. (4.6) and (4.9) give $\chi(r)$ and $\chi'(r)$ at the origin. Finally, the integral of $r^2\chi(r)$ in the interval $0 \le r \le 1$ is determined by Eq. (4.15). Since there are seven constraints we can approximate $\chi(r)$ for $r \le 1$ by a polynomial of sixth degree:

$$
\begin{aligned}
\chi_{\mathrm{poly}}(r) = \frac{\pi^2}{36}&\left[\alpha_0 + \alpha_1(r - 1) + \alpha_2(r - 1)^2\right.\\
&\left.+\alpha_3(r - 1)^3 + (r - 1)^4\left(\beta_0 + \beta_1 r + \beta_2 r^2\right)\right].
\end{aligned}
$$
(4.17)

In this equation, the constants $\alpha_0 = (36/\pi^2)\chi(1)$, $\alpha_1 = (36/\pi^2)\chi'(1)$, $\alpha_2 = (36/\pi^2)\chi''(1)/2$, and $\alpha_3 =$

$(36/\pi^2)\chi'''(1)/6$ are obtained from Eqs. (4.1)–(4.4). From Eqs. (4.6) and (4.9) one gets

$$
\beta_0 = \frac{1}{459}\left(\frac{4309b_4^{\mathrm{HS}}}{3} - \frac{129317}{6} - \frac{10784\sqrt{2}}{\pi}\right), \tag{4.18}
$$

$$
\beta_1 = \frac{1}{27}\left(\frac{554b_4^{\mathrm{HS}}}{3} - \frac{8663}{3} - \frac{1120\sqrt{2}}{\pi}\right). \tag{4.19}
$$

Finally, application of (4.15) yields

$$
\beta_2 = \frac{1}{3}\left(\frac{3803b_4^{\mathrm{HS}}}{6} - \frac{134713}{12} - \frac{920\sqrt{2}}{\pi}\right). \tag{4.20}
$$

The second derivative at the origin is

$$
\begin{aligned}
\chi''_{\mathrm{poly}}(0) &= \frac{\pi^2}{36}\frac{10}{459}\left(\frac{55069b_4^{\mathrm{HS}}}{3} - \frac{981592}{3} - \frac{22232\sqrt{2}}{\pi}\right)\\
&\simeq -\frac{\pi^2}{36}2.07929.
\end{aligned}
$$
(4.21)

In contrast, the exact result is (see the Appendix)

$$
\chi''(0) = -\frac{\pi^2}{36}\left(12 - \frac{18\sqrt{3}}{\pi}\right) \simeq -\frac{\pi^2}{36}2.07608. \tag{4.22}
$$

Therefore, $\chi''_{\mathrm{poly}}(0)/\chi''(0) \simeq 1.00155$. This gives an idea of the extreme accuracy of $\chi_{\mathrm{poly}}(r)$. In fact, we have evaluated numerically $\chi(r)$ by MC integration with 6 significant figures and have found that $\chi_{\mathrm{poly}}(r)$ agrees with $\chi(r)$ within the error bars (see Table I). One could exploit the exact knowledge of $\chi''(0)$, Eq. (4.22), to propose an approximation presumably even more accurate than Eq. (4.17), but this does not seem to be necessary in view of Table I.

V. COMPARISON WITH THE HNC AND PY THEORIES

Once we have obtained the exact temperature-dependence of the function $y_2(r)$ and the associated fourth virial coefficient b_4 for PS, it is worthwhile comparing these two quantities with the predictions provided by the two classical integral equation theories, namely the HNC and PY theories.

A. Cavity function to second order, $y_2(r)$

In the HNC theory, the elementary diagrams are neglected at any order in density [25]. To second order in density, the only elementary diagram is the last one given in Eq. (3.2). Therefore, the function $y_2(r)$ is approximated by

$$
y_2^{\mathrm{HNC}}(r|T^*) = x^3\varphi(r) + 2x^4\psi(r) + \frac{x^4}{2}\gamma^2(r). \tag{5.1}
$$

TABLE I: Values of $-(36/\pi^2)\chi(r)$ in the interval $0 \leq r \leq 1$ as obtained numerically by MC integration and as given by the polynomial approximation (4.17). The number enclosed between parentheses in the second column indicates the 95%-confidence error.

r	MC	Eq. (4.17)
0.00	29.9994(6)	30
0.05	28.5029(5)	28.5031
0.10	27.0146(5)	27.0144
0.15	25.5367(4)	25.5369
0.20	24.0735(4)	24.0736
0.25	22.6277(4)	22.6275
0.30	21.2015(3)	21.2017
0.35	19.7987(3)	19.7991
0.40	18.4228(3)	18.4228
0.45	17.0756(3)	17.0758
0.50	15.7614(2)	15.7612
0.55	14.4822(2)	14.4820
0.60	13.2414(2)	13.2413
0.65	12.0420(2)	12.0421
0.70	10.88745(13)	10.88740
0.75	9.78032(12)	9.78037
0.80	8.72413(14)	8.72404
0.85	7.72152(10)	7.72151
0.90	6.77582(8)	6.77586
0.95	5.89018(7)	5.89019
1.00	5.06759(5)	5.06762

In the PY approximation, apart from the elementary diagrams, a subset of the remaining diagrams is also neglected. In particular, the PY expression for $y_2(r)$ only retains the two first diagrams in Eq. (3.2), so that

$$y_2^{\mathrm{PY}}(r|T^*) = x^3\varphi(r) + 2x^4\psi(r). \qquad (5.2)$$

Figure 1 compares the exact function $y_2(r)$ with the HNC and PY approximations at $T^* = 0$ (hard spheres), $T^* = 1$, and $T^* = 2$. Both theories agree very well with the exact $y_2(r)$ for $r \geq 1.5$ but discrepancies are apparent for shorter distances, especially inside the core ($r < 1$). Although restricted to low densities, Fig. 1 clearly illustrates some of the general features found at finite densities [13, 14]: the HNC overestimates the penetrability effect, while the PY approximation underestimates it. The former property is a consequence of the neglect of $(x^5/2)\chi(r)$, which is a negative definite quantity. This is only partially compensated by the PY neglect of $(x^4/2)\gamma^2(r)$, since $\gamma^2(r) > |\chi(r)|$ for $r < 1$ and, moreover, $x^4 \geq x^5$. While the PY theory tends to be better at lower temperatures (i.e., when the overlapping of particles is hindered and the system is close to that of HS), the HNC is preferable at higher temperatures. If we characterize the quality of each approximation by the separation of the corresponding contact value $y_2(1)$

from the exact result, it turns out that the temperature beyond which the HNC approximation becomes better than the PY approximation is $T^* \simeq 1.04$. This is similar to the behavior found in the one-dimensional case [21].
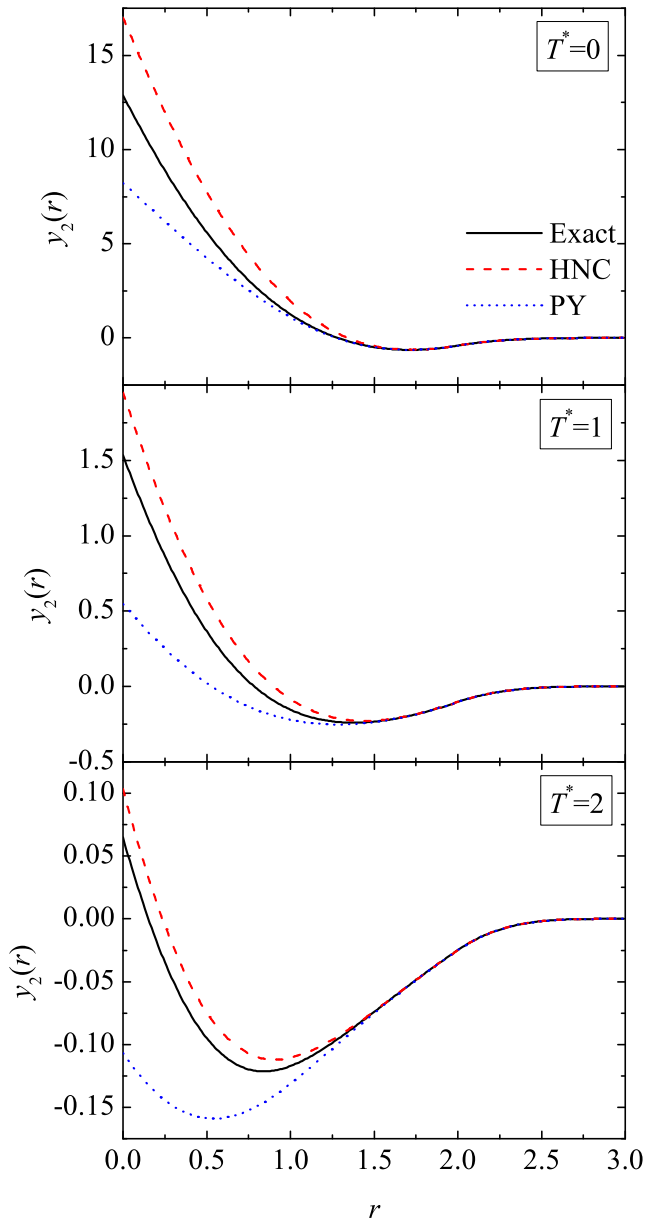

FIG. 1: (Color online) Plot of the function $y_2(r)$ at $T^* = 0$ (top panel), $T^* = 1$ (middle panel), and $T^* = 2$ (bottom panel). The solid lines are the exact results, the dashed lines are the HNC predictions, and the dotted lines are the PY predictions.

B. Fourth virial coefficient

The knowledge of $y_2^{\mathrm{HNC}}(r|T^*)$ and $y_2^{\mathrm{PY}}(r|T^*)$ allows one to get the associated expressions for the fourth virial

TABLE II: Fourth virial coefficient $b_4(T^*)$ and other related quantities as given exactly and by the HNC and PY approximations through the virial (v), energy (e), and compressibility (c) routes.

Theory	$b_4(T^*)$	$b_4(0)$	T_0^*	$T_{\min}^*$	$b_4\|_{\min}$
Exact	$x^4[b_4^{\mathrm{HS}}x^2 - (1-x)(4352 - 1995x)/70]$	b_4^{HS}	0.7250	1.1027	-1.4803
HNC,v/e	$x^4(6347x - 4352)/70$	$\frac{57}{2}$	0.8641	1.2574	-1.1258
HNC,c	$x^4(31735x - 26112)/420$	$\frac{5623}{420}$	0.5778	0.9314	-2.3345
PY,v	$16x^4(171x - 136)/35$	16	0.6304	0.9888	-2.0378
PY,e	$2x^4(6347x - 5440)/175$	$\frac{1814}{175}$	0.5140	0.8641	-2.7485
PY,c	$x^4(6347x - 4352)/105$	19	0.8641	1.2574	-0.7505

coefficient $b_4(T^*)$. As discussed in Section II, there are three alternative routes [cf. Eqs. (2.11)–(2.13)] and there is no reason to expect internal consistency among them, unless the exact $y_2(r)$ is used. The expressions for $b_4^v(T^*)$, $b_4^e(T^*)$, and $b_4^c(T^*)$ in the HNC and PY approximations are given in Table II, where, for completeness, the exact expression, Eq. (4.13), is also included. It is known [29] that the HNC integral equation provides thermodynamically consistent results through the virial and energy routes, regardless of the potential considered. This explains the fact that $b_4^{\mathrm{HNC},v}(T^*) = b_4^{\mathrm{HNC},e}(T^*)$. On the other hand, the PY integral equation yields three different predictions, i.e., $b_4^{\mathrm{PY},v}(T^*) \neq b_4^{\mathrm{PY},e}(T^*) \neq b_4^{\mathrm{PY},c}(T^*)$. It is interesting to note that $b_4^{\mathrm{HNC},v/e}(T^*) = \frac{3}{2}b_4^{\mathrm{PY},c}(T^*) = \frac{1}{4}x db_4^{\mathrm{PY},e}(T^*)/dx$.

In the limit $T^* \to 0$ one recovers the known results for HS, namely $b_4^{\mathrm{HNC},v/e}(0) = \frac{57}{2} = 28.5$, $b_4^{\mathrm{HNC},c}(0) = \frac{5623}{420} \simeq 13.3881$, $b_4^{\mathrm{PY},v}(0) = 16$, and $b_4^{\mathrm{PY},c}(0) = 19$. Although the energy route is ill defined for strict HS, taking the zero-temperature limit on the PS model yields well defined values [30]. In that way, one finds $b_4^{\mathrm{PY},v}(0) = \frac{1814}{175} \simeq 10.3657$, which is a rather poor value reflecting the inaccuracy at any temperature of $y_2^{\mathrm{PY}}(r)$ for $r < 1$. In the opposite high-temperature limit, one has $\lim_{T^* \to \infty} b_4(T^*)/x^4 = -2176/35$. This exact value is retained by all the approximations, except by the compressibility route in the PY theory, which yields $\lim_{T^* \to \infty} b_4^{\mathrm{PY},c}(T^*)/x^4 = -4352/105$, i.e., 2/3 of the exact result.

While $b_2(T^*)$ and $b_3(T^*)$ are positive definite quantities, this is not the case of $b_4(T^*)$. The latter quantity changes sign at a certain "Boyle-like" temperature T_0^*. In addition, $b_4(T^*)$ presents a (negative) minimum value $b_4\|_{\min}$ at a temperature $T_{\min}^* > T_0^*$. The numerical values of T_0^*, $T_{\min}^*$, and $b_4\|_{\min}$ are displayed in Table II. From Eq. (2.12) one can see that the temperature $T_{\min}^*$ associated with $b_4^e(T^*)$ is the temperature across which the integral $\int_0^1 dr\, r^2 y_2(r|T^*)$, and hence the third-order term in the density expansion of the internal energy, changes from positive to negative.

The temperature dependence of the fourth virial coefficient is shown in Fig. 2, where, apart from the exact curves, the two HNC approximations and the three PY
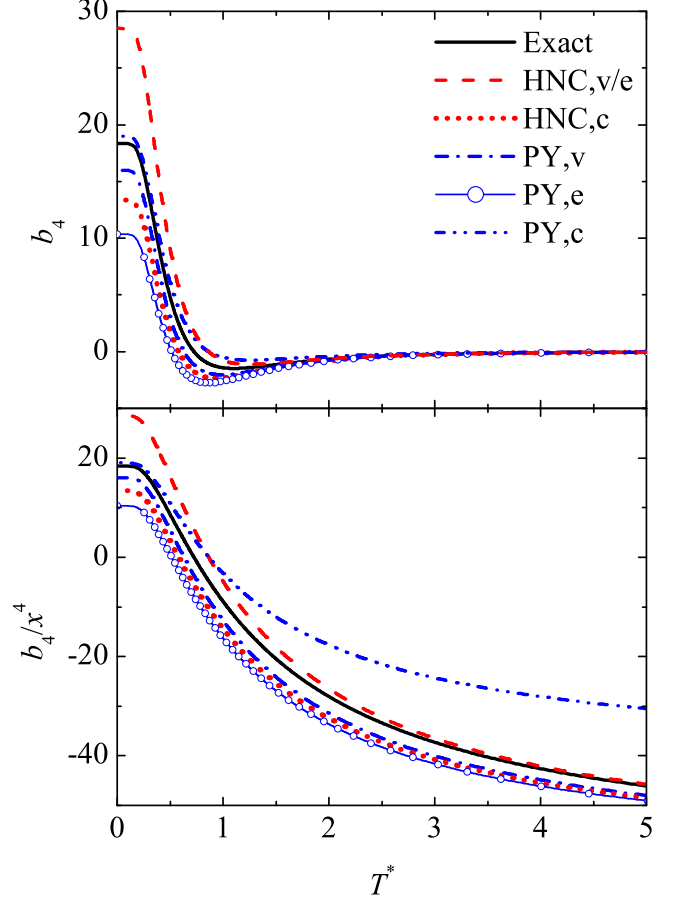

FIG. 2: (Color online) Plot of the fourth virial coefficient $b_4(T^*)$ (top panel) and of the scaled fourth virial coefficient $b_4(T^*)/x^4$ (bottom panel), where $x = 1 - e^{-1/T^*}$, as given exactly and by the HNC and PY approximations.

approximations are included. The best approximation up to $T^* \simeq 0.71$ is provided by $b_4^{\mathrm{PY},c}$. In the intermediate range $0.71 \lesssim T^* \lesssim 1.04$, however, $b_4^{\mathrm{PY},v}$ presents the best agreement. Finally, for $T^* \gtrsim 1.04$ the best performance corresponds to $b_4^{\mathrm{HNC},v/e}$. Within the PY theory, the energy route is never better than the virial route but becomes preferable to the compressibility route for $T^* \gtrsim 1.22$. In the case of the HNC theory, the compress-

ibility route is better than the virial/energy routes for $T^* \lesssim 0.73$ only.

VI. CONCLUSION

In this paper we have considered a three-dimensional fluid of particles interacting via the PS interaction (1.1). This potential encompasses the ideal gas in the high-temperature limit ($T^* \to \infty$ or $x \to 0$) and the HS fluid in the low-temperature limit ($T^* \to 0$ or $x \to 1$). However, at finite temperature the problem becomes much more difficult. Even the one-dimensional case is not exactly solvable [21] since there is no *a priori* limitation to the number of particles that can interact simultaneously with a given particle.

The diagrams which appear in the density expansions for the PS fluids are exactly the same as those appearing for HS fluids, except that each diagram needs to be multiplied by the temperature-dependent parameter x raised to the number of bonds. By exploiting this fact, we have obtained the cavity function through second order in density and the equation of state through the fourth virial coefficient. In order to obtain $y_2(r|T^*)$, we have needed to extend to $r < 1$ the functions evaluated by Nijboer and van Hove [22] for $r > 1$. Nevertheless, the possible analytical evaluation of the elementary-diagram function $\chi(r)$ for $r < 1$ seems to be a formidable task. Thus, we have resorted in that case to two complementary approaches: (i) a numerical computation by MC integration with an error bar of the order of 0.001% and (ii) a sixth-degree polynomial approximation constructed by enforcing seven exact constraints. Both methods show such an excellent mutual agreement that the results obtained from the polynomial approximation can be considered as exact from a practical point of view.

The results obtained here for $y_2(r|T^*)$ and $b_4(T^*)$ have been compared with those corresponding to the two classical integral equation theories, namely the HNC and PY theories. It is known that the PY theory is much better than the HNC one for HS fluids, so that one could have expected a similar situation for PS fluids, at least at low temperatures. Our results show that this is indeed the case, provided that $T^* \lesssim 1$. However, even at very low temperatures (including the HS limit $T^* \to 0$), the PY solution strongly underestimates the cavity function in the overlapping region. This reflects the fact that the fortunate practical cancelation (in the case of HS) of the diagrams neglected by the PY equation does not apply for $r < 1$. In this respect, it is interesting to note that the widely extended belief that the PY theory becomes exact in the special case of one-dimensional hard rods is only correct for $r > 1$ [21].

When comparing the exact fourth virial coefficient with the HNC and PY theories one has to take into account their thermodynamic inconsistency, yielding two HNC predictions (virial/energy and compressibility routes) and three PY predictions (virial, energy, and compressibility routes). All these predictions capture the non-monotonic behavior of $b_4(T^*)$. In both theories, the compressibility route is the best one for $T^* \lesssim 0.7$, while the virial route is preferable if $T^* \gtrsim 0.7$. As in the case of the structural functions, the equation of state is better described by the HNC equation than by the PY equation for high enough temperatures ($T^* \gtrsim 1$).

It is obvious that access to non-trivial exact information on the structural and thermodynamic properties of fluids, even if restricted to special cases, is of paramount importance. From that point of view, we hope that the results reported in this paper can contribute to an advancement on our knowledge of the behavior of systems of particles interacting through bounded potentials.

APPENDIX: EVALUATION OF $\chi''(0)$

The function $\chi(r)$ is represented by the elementary diagram displayed at the end of the right-hand side of Eq. (3.2). Thus,

$$\chi(r_2) = \int d\mathbf{r}_3 \int d\mathbf{r}_4 f(r_3) f(r_4) f(r_{23}) f(r_{24}) f(r_{34}), \tag{A.1}$$

where here $f(r) = f_{HS}(r) = -\Theta(1 - r)$. Now we differentiate with respect to r_2 and take into account the mathematical property

$$\frac{\partial f(r_{23})}{\partial r_2} = \delta(r_{23} - 1) \frac{\partial r_{23}}{\partial r_2} = \delta(r_{23} - 1) \frac{\mathbf{r}_2 \cdot \mathbf{r}_{23}}{r_2}. \tag{A.2}$$

The result is

$$\begin{aligned} \chi'(r_2) &= 2 \int d\mathbf{r}_3 \int d\mathbf{r}_4 f(r_3) f(r_4) f(r_{24}) f(r_{34}) \\ &\quad \times \delta(r_{23} - 1) \cos\theta_{23}, \end{aligned} \tag{A.3}$$

where θ_{23} is the polar angle of the vector $\mathbf{r}_{23}$ and the z axis is assumed to point in the direction of $\mathbf{r}_2$. Making

the change of variables $\mathbf{r}_3 \to \mathbf{r}_{23}$, $\mathbf{r}_4 \to \mathbf{r}_{24}$, Eq. (A.3) becomes

$$\chi'(r_2) = 2 \int d\mathbf{r}_3 \int d\mathbf{r}_4 f(r_{23}) f(r_{24}) f(r_4) f(r_{34})$$
$$\times \delta(r_3 - 1) \cos\theta_3. \quad (A.4)$$

Note that $r_{23}^2 = r_2^2 + 1 - 2r_2 \cos\theta_3$, so that a necessary (but not sufficient) condition for $f(r_{23}) \neq 0$ is $\theta_3 < \pi/2$. Therefore, in the limit $r_2 \to 0$, one has

$$\chi'(0) = 4\pi\gamma(1) \int_0^{\pi/2} d\theta_3 \sin\theta_3 \cos\theta_3 = \frac{\pi^2}{36} 30, \quad (A.5)$$

in agreement with Eq. (4.9).

Now we differentiate again with respect to r_2 to get

$$\chi''(r_2) = \chi_1''(r_2) + \chi_2''(r_2), \quad (A.6)$$

where

$$\chi_1''(r_2) = 2 \int d\mathbf{r}_3 \int d\mathbf{r}_4 f(r_{24}) f(r_4) f(r_{34})$$
$$\times \delta(r_3 - 1) \cos\theta_3 \delta(r_{23} - 1) \cos\theta_{23}, \quad (A.7)$$

$$\chi_2''(r_2) = 2 \int d\mathbf{r}_3 \int d\mathbf{r}_4 f(r_{23}) f(r_4) f(r_{34})$$
$$\times \delta(r_3 - 1) \cos\theta_3 \delta(r_{24} - 1) \cos\theta_{24}. \quad (A.8)$$

Let us first consider $\chi_1''(r)$. Note that $\cos\theta_{23} = r_2 - \cos\theta_3$, where it has been taken into account that $r_3 = 1$. Now, using the property

$$\delta(h(x)) = |h'(x_0)|^{-1} \delta(x - x_0), \quad (A.9)$$

where $h(x)$ is a function that vanishes at $x = x_0$, we have

$$\delta(r_{23} - 1) = r_2^{-1} \delta(\cos\theta_3 - r_2/2). \quad (A.10)$$

Thus,

$$\chi_1''(r_2) = 2r_2 \int_0^{2\pi} d\phi_3 \int d\mathbf{r}_4 f(r_{24}) f(r_4) f(r_{34}), \quad (A.11)$$

where $r_{34}^2 = r_4^2 + 1 - r_4[r_2 \cos\theta_4 + \sqrt{4 - r_2^2} \sin\theta_4 \cos(\phi_3 - \phi_4)]$, ϕ_3 and ϕ_4 being azimuthal angles. At the origin one simply has

$$\chi_1''(0) = 0. \quad (A.12)$$

In Eq. (A.8), since $r_4^2 = r_2^2 + 1 - 2r_2 \cos\theta_{24}$, a necessary condition for $f(r_4) \neq 0$ is $\theta_{24} < \pi/2$. Now, setting $r_2 = 0$ and taking into account that $\cos\theta_{24} \to -\cos\theta_4$, Eq. (A.8) becomes

$$\chi_2''(0) = -2 \int_0^{2\pi} d\phi_3 \int_0^{2\pi} d\phi_4 \int_0^1 d(\cos\theta_3) \cos\theta_3$$
$$\times \int_{-1}^0 d(\cos\theta_4) \cos\theta_4 f(r_{34}), \quad (A.13)$$

where now $r_{34}^2 = 2[1 - \cos\theta_3 \cos\theta_4 - \sin\theta_3 \sin\theta_4 \cos(\phi_3 - \phi_4)]$. The changes $z = \cos\theta_3$, $z' = -\cos\theta_4$, and $\phi = \phi_3 - \phi_4$ lead to

$$\chi_2''(0) = -8\pi \int_0^1 dz \int_0^1 dz' zz' \int_0^\pi d\phi$$
$$\times \Theta\left(\cos\phi - \frac{1 + 2zz'}{2\sqrt{(1 - z^2)(1 - z'^2)}}\right) \quad (A.14)$$

It can be easily seen that $1 + 2zz' < 2\sqrt{(1 - z^2)(1 - z'^2)}$ if and only if $z^2 + z'^2 + zz' < 3/4$. This requires that $0 < z < \sqrt{3/2}$ and $0 < z' < (\sqrt{3(1 - z^2)} - z)/2$. Consequently,

$$\chi_2''(0) = -8\pi \int_0^{\sqrt{3}/2} dz \int_0^{(\sqrt{3(1-z^2)}-z)/2} dz' zz'$$
$$\times \cos^{-1} \frac{1 + 2zz'}{2\sqrt{(1 - z^2)(1 - z'^2)}}. \quad (A.15)$$

The result of the integral is

$$\chi_2''(0) = -\frac{\pi^2}{36}\left(12 - \frac{18\sqrt{3}}{\pi}\right). \quad (A.16)$$

[1] C. N. Likos, Phys. Rep. **348**, 267 (2001).
[2] C. N. Likos, H. Löwen, M. Watzlawek, B. Abbas, O. Jucknischke, J. Allgaier, and D. Richter, Phys. Rev. Lett. **80**, 4450 (1998); M. Watzlawek, C. N. Likos, and H. Löwen, *ibid.* **82**, 5289 (1999).
[3] F. H. Stillinger and D. K. Stillinger, Physica A **244**, 358 (1997).
[4] H. Graf and H. Löwen, Phys. Rev. E **57**, 5744 (1998).
[5] A. Lang, C. N. Likos, M. Watzlawek, and H. Löwen, J. Phys.: Condens. Matter **12**, 5087(2000).
[6] A. A. Louis, P. G. Bolhuis, and J.-P. Hansen, Phys. Rev. E **62**, 7961 (2000).
[7] C. N. Likos, A. Lang, M. Watzlawek, and H. Löwen, Phys. Rev. E **63**, 031206 (2001).

[8] R. Finken, J.-P. Hansen, and A. A. Louis, J. Stat. Phys. **110**, 1015 (2003).

[9] C. Marquest and T. A. Witten, J. Phys. (France) **50**, 1267 (1989).

[10] W. Klein, H. Gould, R. A. Ramos, I. Clejan, and A. I. Mel'cuk, Physica A **205**, 738 (1994).

[11] C. N. Likos, M. Watzlawek, and H. Löwen, Phys. Rev. E **58**, 3135 (1998).

[12] M. Schmidt, J. Phys.: Condens. Matter **11**, 10163 (1999).

[13] M. J. Fernaud, E. Lomba, and L. L. Lee, J. Chem. Phys. **112**, 810 (2000).

[14] Y. Rosenfeld, M. Schmidt, M. Watzlawek, and H. Löwen, Phys. Rev. E **62**, 5006 (2000).

[15] M. Schmidt and M. Fuchs, J. Chem. Phys. **117**, 6308 (2002).

[16] S.-C. Kim and S.-Y. Suh, J. Chem. Phys. **117**, 9880 (2002).

[17] N. Choudhury and S. K. Ghosh, J. Chem. Phys. **119**, 4827 (2003).

[18] L. Acedo and A. Santos, Phys. Lett. A **323**, 427 (2004).

[19] A. Santos, "Kinetic Theory of Soft Matter. The Penetrable-Sphere Model," in *Rarefied Gas Dynamics: 24th International Symposium on Rarefied Gas Dynamics*, edited by M. Capitelli (AIP Conference Proceedings **762**, 2005), pp. 276–281; cond-mat/0501068.

[20] R. L. C. Vink and M. Schmidt, Phys. Rev. E **71**, 051406 (2005).

[21] Al. Malijevský and A. Santos, J. Chem. Phys. **124**, 074508 (2006).

[22] B. R. A. Nijboer and L. van Hove, Phys. Rev. **85**, 777 (1952).

[23] R. Balescu, *Equilibrium and Nonequilibrium Statistical Mechanics* (Wiley, New York, 1974).

[24] J. A. Barker and D. Henderson, Rev. Mod. Phys. **48**, 587 (1976).

[25] J.-P. Hansen and I. R. McDonald, *Theory of Simple Liquids*, (Academic Press, London, 1986).

[26] S. Labík, H. Gabrielová, J. Kolafa, and A. Malijevský, Mol. Phys. **101**, 1139 (2003).

[27] L. L. Lee, J. Chem. Phys. **103**, 9388 (1995); L. L. Lee, D. Ghonasgi, and E. Lomba, *ibid.* **104**, 8058 (1996); L. L. Lee and A. Malijevský, *ibid.* **114**, 7109 (2001).

[28] To the best of our knowledge, Eqs. (4.12) and (4.13) were first derived by K. Hiroike, J. Phys. Soc. Jpn. **12**, 326 (1957).

[29] T. Morita, Progr. Theor. Phys. **23**, 829 (1960); see also Ref. [24], p. 636.

[30] It is interesting to note that the HS limit of the energy-route equation of state may depend in general on the interaction potential used as a starting point. In this respect, see A. Santos, J. Chem. Phys. **123**, 104102 (2005); Mol. Phys., in press, preprint cond-mat/0607126.